Oxidation Catalysis

DOI: 10.1002/ange.201405232

Catalytic Consequences of the Thermodynamic Activities at Metal Cluster Surfaces and Their Periodic Reactivity Trend for Methanol Oxidation**

*Weifeng Tu and Ya-Huei (Cathy) Chin**

Abstract: *The periodic reactivity trend and the connection of kinetics to the thermodynamic activity of oxygen are established for the oxidation of methanol on metal clusters. First-order rate coefficients are a single-valued function of the O_2-to-CH_3OH ratio, because this ratio, together with the rate constants for O_2 and CH_3OH activation, determine the oxygen chemical potential, thus the relative abundance of active sites and bulk chemical state of the clusters. CH_3OH activation rate constants on oxygen-covered Ag, Pt, and Pd and on RuO_2 clusters vary with the metal–oxygen binding strength in a classical volcano-type relation, because the oxygen-binding strength directly influences the reactivities of oxygen as H abstractors during the kinetically relevant CH_3OH activation step. The differences in oxygen thermodynamic activity lead to five orders of magnitude variation in rates ($Pt > Pd > RuO_2 > Ag$, 373 K), because of its strong effects on the activation enthalpy and more prominently activation entropy in CH_3OH activation.*

The direct relation between chemical potentials at catalytic surfaces and their reactivities has been recognized for oxidation,[1] dehydrogenation,[2] and ammonia synthesis[3] reactions. Reactivities during oxidation reactions (CH_4 on Pt[1a] and Pd;[1c,d] C_2H_6 on Pt;[1b] NO on Pt,[1e] Pd,[1f] Rh,[1g] and Co;[1g] CH_3OCH_3 on Pt, Pd, and Rh;[1h] CO on Au[1i] and Pt[1j–l]) on metal or oxide clusters vary strictly with the instantaneous oxygen chemical potential at cluster surfaces, as it dictates the relative abundances of chemisorbed oxygen and metal site and the thermodynamic tendency for clusters to tether between metal and oxide states.[1c,f,4] Chemical potentials at catalytic surfaces are unique to the specific reaction system because their instantaneous values are given by the kinetic coupling of oxidant (O_2) and reductant (CH_4, C_2H_6, CH_3OCH_3, or CO) activation steps, as these steps form and remove surface species, thus dictating the relative surface abundances and local thermodynamic activities, as previously established.[1] Oxygen chemical potentials at metal cluster surfaces are a strict function of the rate constants for the activation of oxidant and reductant and their pressures.[1a,b] The oxygen chemical potentials become independent of these rate constants in the limiting case of quasi-equilibrated oxidant activation; instead, their values and the coverages of oxygen atoms depend strictly on the equilibrium constant and the pressures of chemical species involved in generating the reactive oxygen intermediates.[1c–g] Previously established examples for this limiting condition include: 1) CH_4–O_2 reactions on Pd or PdO,[1c,d] during which the oxygen chemical potentials vary with the equilibrium constant for O_2 dissociation and O_2 pressure and 2) NO–O_2 reactions on Pt, Pd, Rh, or Co,[1e–g] which vary with the equilibrium constant for NO-to-NO_2 interconversion and NO_2-to-NO ratio.

Oxidative dehydrogenation of CH_3OH is a specific class of oxidation reactions that use molecular oxygen to catalytically transform CH_3OH on metal or metal-oxide clusters to a broad range of value-added, oxygen-containing products (for example, HCHO, $HCOOCH_3$, and sequentially to $CH_3OCH_2OCH_3$). The catalytic rates, their connection with the thermodynamic activities of surface oxygen species, and the periodic reactivity trend have, however, not been established. Here, we report the mechanistic synergy and a generalized connection between the first-order rate coefficients and operating oxidant-to-reductant ratios for methanol oxidative dehydrogenation, which forms CO_2, HCHO, $HCOOCH_3$, and H_2O on Ag, Pt, Pd, and Ru clusters (in either metal or oxide state). First-order rate coefficients for CH_3OH oxidative dehydrogenation (ODH) are defined as the methanol turnover rates ($r_{ODH,M,i}$, per exposed metal site, subscript *M* denotes Ag, Pt, Pd, or Ru; subscript *i* denotes kinetic regime *i*, $i = 1$, 2, or 3) divided by methanol pressure and denoted as $k^{1st}_{ODH,M,i}$ [Eq. (1)]:

$$k^{1st}_{ODH,M,i} = \frac{r_{ODH,M,i}}{[CH_3OH]} \quad (1)$$

Their values on Ag, Pt, Pd, and Ru clusters (average diameter: 2.8–3.2 nm, measured at a reduced state) are a single-valued function (*f*) of O_2-to-CH_3OH ratios [$k^{1st}_{ODH,M,i} = f(O_2/CH_3OH)$], irrespective of the specific O_2 and CH_3OH pressures, as shown in Figure 1. Selectivities of carbon-containing products (CO_2, HCHO, and $HCOOCH_3$) during CH_3OH-O_2 reactions also vary with the O_2-to-CH_3OH ratios. The selectivity dependencies for each species, however, differ among the metals, because the relative rates of primary and secondary reactions are influenced to different extents by both the O_2-to-CH_3OH ratio[5] and oxygen–metal bond strength. The generalized relation in Figure 1 reflects the direct, macroscopic relation between kinetic properties (rate coefficients) and thermodynamic quantities, namely the

[*] Dr. W. Tu, Prof. Y.-H. Chin
Department of Chemical Engineering and Applied Chemistry
University of Toronto, Toronto, Ontario (Canada)
E-mail: cathy.chin@utoronto.ca
Homepage: http://www.labs.chem-eng.utoronto.ca/catalysis/

[**] This study was supported by Natural Sciences and Engineering Research Council of Canada and Canada Foundation for Innovation.

Supporting information for this article is available on the WWW under http://dx.doi.org/10.1002/anie.201405232.

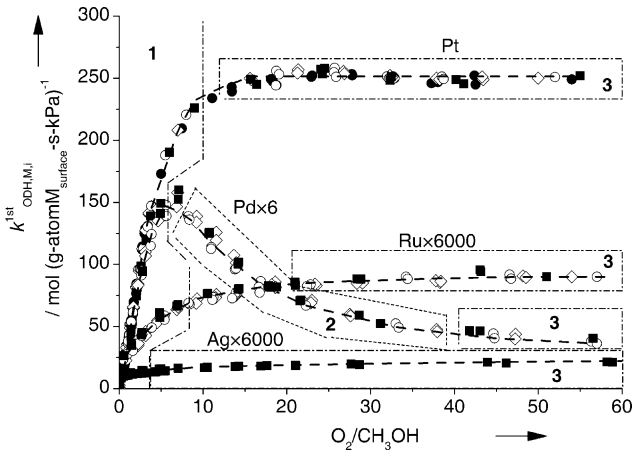

Figure 1. First-order rate coefficients ($k^{1st}_{ODH,M,i} = r_{ODH,M,i}[CH_3OH]^{-1}$, M = Ag, Pt, Pd, or Ru) for CH_3OH oxidative dehydrogenation (ODH) at 373 K on Ag, Pt, Pd, and Ru clusters (1.0 wt% metal on SiO_2, 2.8–3.2 nm mean metal cluster diameters) as a single-valued function of O_2-to-CH_3OH ratio. The CH_3OH pressure are 1.75 (●), 1.5 (◇), 1.25 (○), and 1 kPa (■). (2.52×10^4 cm^3 (g_{cat}-h)$^{-1}$ for Ag, 1.26×10^8 cm^3 (g_{cat}-h)$^{-1}$ for Pt and Pd, 1.26×10^5 cm^3 (g_{cat}-h)$^{-1}$ for Ru; kinetic regimes 1, 2, and 3 for CH_3OH oxidative dehydrogenation are labeled as **1**, **2**, and **3**, respectively).

oxygen chemical potentials at catalytic sites prescribed by the operating O_2-to-CH_3OH ratio and the rate constants for oxygen and methanol activation. Similar relations connecting reactivities to the free energies of adsorbates have been proposed for methanol electrooxidation[6] based on density functional theory study. The binding energies of adsorbates on metal surfaces and the activation barriers for methanol dehydrogenation[7] or oxygen dissociation[8] have also been calculated and shown to follow a Brønsted-Evans-Polanyi-type relation. Our findings, however, provide the direct, experimental evidence of a generalized relation between kinetic and thermodynamic properties. This relation, denoted here as the "kinetic phase diagram" (Figure 1), provides the reactivity trend connecting catalytic behavior to the instantaneous thermodynamic activities and is applicable irrespective of metal identity, chemical state, differences in exposed facets, and variation in binding strengths for the case of irreversible oxygen activation.

During steady-state methanol oxidation, the oxidant-to-reductant ratio determines the relative abundances of chemisorbed oxygen atoms (O*) and unoccupied metal sites (*) at cluster surfaces, derived from Equation (2):

$$\frac{dO^*}{dt} = 0 = \nu_{O_2} r_{O_2,f} - \nu_{O_2} r_{O_2,r} - \nu_{CH_3OH} r_{CH_3OH} \quad (2)$$

where $r_{O_2,f}$ and $r_{O_2,r}$ denote the forward and reverse rates of O_2 activation, respectively, and r_{CH_3OH} denotes the CH_3OH activation rates. ν_{O_2} and ν_{CH_3OH} are the stoichiometric coefficients for O_2 and CH_3OH activation (ν_{O_2} =2 and ν_{CH_3OH} depend on the number of O* involved in methanol activation), respectively. Equation (3) gives the relative abundance of oxygen-to-metal sites ([O*]/[*]) as a function (g) of the rate constants for oxygen activation $(k_{O_2,f})$, O* recombination $(k_{O_2,r})$, and methanol dissociation (k_{CH_3OH}) and the partial pressures of oxygen ([O_2]) and methanol ([CH_3OH]) (see derivation in Section S.1 in the Supporting Information):

$$\frac{[O^*]}{[*]} = g(k_{O_2,f}, k_{O_2,r}, k_{CH_3OH}, [CH_3OH], [O_2]) \quad (3)$$

which simplifies to Equation (4),

$$\frac{[O^*]}{[*]} = \left(\frac{k_{O_2,f}[O_2]}{k_{CH_3OH}[CH_3OH]}\right)^{0.5} = g\left(\frac{[O_2]}{[CH_3OH]}\right) \quad (4)$$

when CH_3OH activation on an O* atom pair limits rates and O* reaction with CH_3OH occurs at much higher rates than O* recombinative desorption $(r_{O_2,r} \ll r_{CH_3OH})$.

The first-order rate coefficients [$k^{1st}_{ODH,M,i} = r_{ODH,M,i}$-$[CH_3OH]^{-1}$, Eq. (1)] vary with O_2-to-CH_3OH ratios differently in two distinct kinetic regimes on Ag, Pt, and Ru clusters (regimes 1 and 3, as labelled in Figure 1). In regime 1 (O_2-to-CH_3OH ratios of 0.1–4 for Ag, 0.1–9 for Ru, and 0.1–10 for Pt), first-order rate coefficients increase with increasing O_2-to-CH_3OH ratio ($k^{1st}_{ODH,M,1} = k_{M,O_2,f}[O_2][CH_3OH]^{-1}$, $k_{M,O_2,f}$ denotes the oxygen dissociation rate constant on metal M), because oxygen dissociation on metal sites limits catalytic turnovers.[5] As the O_2-to-CH_3OH ratio exceeds a critical value (O_2-to-$CH_3OH \geq 4$, 9, and 10 for Ag, Ru, and Pt, respectively), which corresponds to regime 3, first-order rate coefficients become a constant value ($k^{1st}_{ODH,M,3} = k_{M,[O^*\text{-}O^*]}$, $k_{M,[O^*\text{-}O^*]}$ denotes the rate constant for methanol activation assisted by an oxygen atom pair), during which CH_3OH activation on cluster surfaces with O* coverages either at saturation or do not vary with oxygen chemical potential becomes the kinetically relevant step, as derived elsewhere.[5] On Pd clusters, similar kinetic regimes (O_2-to-CH_3OH ratios of 0–7 and 40–60 for regimes 1 and 3, respectively) and kinetic dependencies are observed but with an additional regime (regime 2) detected between regimes 1 and 3, in which the first-order rate coefficients are inversely proportional to the O_2-to-CH_3OH ratio ($k^{1st}_{ODH,Pd,2} = (k_{Pd,[O^*\text{-}*]})^2$-$(k_{Pd,O_2,f})^{-1}\{[O_2]/[CH_3OH]\}^{-1}$, $k_{Pd,[O^*\text{-}*]}$ denotes methanol activation rate constant on O* and * site-pairs, derived in the Supporting Information in Section S2). These kinetic dependencies in regime 2 are consistent with the predominant involvement of oxygen–oxygen vacancy pairs (O*-*) for CH_3OH activation on Pd cluster surfaces nearly saturated with O*. As a result, the first-order rate coefficients in regime 2 decrease with increasing O_2-to-CH_3OH ratio until the O_2-to-CH_3OH ratio reaches about 40 (regime 3), above which they maintain at a lower, constant value [5 ± 0.5 mol (g-atom $Pd_{surface}$-s-kPa)$^{-1}$, 373 K].

Isothermal volumetric oxygen uptakes (0–30 kPa O_2) at 373 K (Figure 2 and Section S3) were used to determine the extent to which metal clusters covered with O* and ultimately formed bulk oxides at the oxygen chemical potential range used for methanol oxidation. At 373 K, Ag and Pd clusters maintain their metallic bulk with surface metal sites predominantly occupied by O* ($O^*_{saturation}/M_{surface} = 0.84 \pm 0.05$ and 1.00 ± 0.05 for Ag and Pd clusters, which correspond to

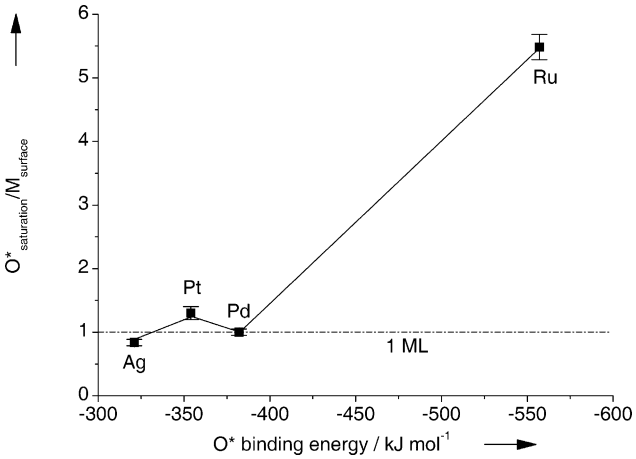

Figure 2. The atomic ratios of oxygen to exposed metal ($O^*_{saturation}/M_{surface}$, M = Ag, Pt, Pd, Ru) at the limit of oxygen saturation at 373 K, extracted from isothermal oxygen uptakes (0–30 kPa O_2) on Ag, Pt, Pd, and Ru clusters of 2.8—3.2 nm average diameters, are plotted against the DFT-calculated O* binding energy on closed packed metal surfaces.[9] See Section S.3 for the oxygen uptake isotherms.

$O^*_{saturation}/M_{total}$ of 0.31 and 0.33, respectively; $O^*_{saturation}$, $M_{surface}$, M_{total} denote the number of O* atoms at surface saturation, the number of exposed metal atoms, and the number of total metal atoms, respectively) for O_2 pressures up to 30 kPa without the concurrent presence of methanol. Under these conditions, Pt cluster surfaces are saturated with O* with traces of oxygen dissolved into the cluster bulk ($O^*_{saturation}/Pt_{surface} = 1.3 \pm 0.1$ and $O^*_{saturation}/Pt_{total} = 0.47$). In contrast, the Ru cluster is oxidized above 1.3 kPa O_2 with an atomic oxygen-to-exposed Ru ($O^*_{saturation}/Ru_{surface}$) ratio of 5.5 ± 0.2, which corresponds to an $O^*_{saturation}/Ru_{total}$ of 1.7, approaching the value expected for complete bulk oxidation ($O^*_{saturation}/Ru_{total} = 2$). The bulk RuO_2 formation is consistent with its strong thermodynamic tendency towards oxidation, as predicted from extrapolation of measured phase boundary at 1073–1773 K[10] to occur at 10^{-27} Pa O_2 at 373 K.

As oxygen chemical potentials and O_2-to-CH_3OH ratios increase (Figure 1), the changes in rate coefficient values and their dependencies on the O_2-to-CH_3OH ratio reflect a dynamic shift in the identity of active sites on metallic Ag, Pt, and Pd clusters from uncovered to covered with O* and on Ru as Ru undergoes bulk oxidation. The single-value functional dependence of rate coefficients on the operating O_2-to-CH_3OH ratios in Figure 1, which appears to be general for methanol oxidation catalysis, results from the direct connection between kinetics and the thermodynamic activities at cluster surfaces, the latter determine the availability of reactive oxygen, the nature of active sites, and in turn the identity of the kinetically relevant step.

We establish next the periodic reactivity trend among these metal clusters and interpret the trend in terms of activation enthalpies and entropies. In regime 3, methanol conversion rates remain unchanged with O_2 pressures (the reaction order with respect to oxygen is 0 ± 0.1), thus first-order rate coefficients ($k^{1st}_{ODH,M,3} = k_{M,[O^*\text{-}O^*]}$, M = Ag, Pt, Pd, or Ru, 333–492 K) reflect the reactive collision frequencies of CH_3OH on metal (Ag, Pt, Pd) or oxide (RuO_2) cluster surfaces either saturated with O* or with O* coverages insensitive to changing the O_2-to-CH_3OH ratio. These rate coefficients differ by five orders of magnitude in the decreasing reactivity order of $Pt > Pd > RuO_2 > Ag$, as shown in an Arrhenius plot in Figure 3. Density functional

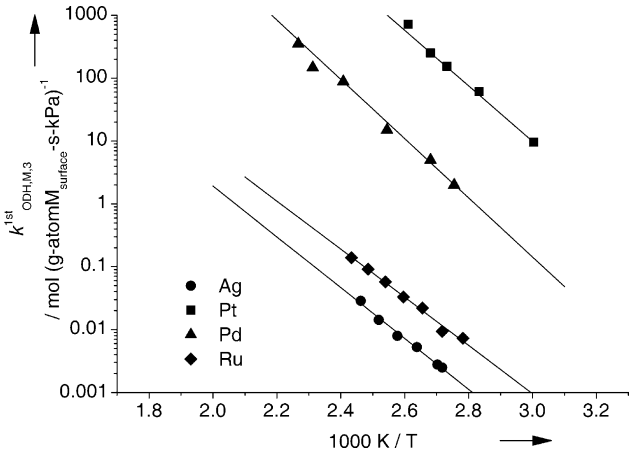

Figure 3. First-order rate coefficients ($k^{1st}_{ODH,M,3} = k_{M,[O^*\text{-}O^*]}$) for CH_3OH oxidative dehydrogenation (ODH) on Ag, Pt, Pd, and Ru clusters (2.8–3.2 nm) in kinetic regime 3 at high O_2-to-CH_3OH ratios (O_2-to-CH_3OH ratios of 20–60 for Ag, 10–60 for Pt, 40–60 for Pd, and 20–60 for Ru). (2.52×10^4 cm^3 (g_{cat}-h)$^{-1}$ for Ag, 1.26×10^8 cm^3 (g_{cat}-h)$^{-1}$ for Pt and Pd, 1.26×10^5 cm^3 (g_{cat}-h)$^{-1}$ for Ru clusters).

theory calculations,[11] temperature-programmed desorption,[12] and Fourier transform infrared reflection absorption spectroscopy[13] on oxygen-covered metal [Ag(211),[11a] Ag-(110),[12a] Cu(211),[11a] Pt(111),[12b] Pt(100),[12c] Pt(211),[11a] Pd-(211),[11a] Rh(211),[11a] and Ru(0001)[13]] or oxide [RuO_2-(110)[11b,14]] surfaces show that O–H bond cleavage is the predominant CH_3OH activation route, as opposed to the case on uncovered metal surfaces, on which either O–H bond [Ag(110),[7] Cu(110),[7,15] Pt(111),[7,16] Pd(111),[7] and Ru-(0001)[13b,17]] or C–H bond [Pt(111)[18] and Pd(111)[19]] scission of CH_3OH may occur. Chemisorbed oxygen atoms may act as a Brønsted base[11a,12] for abstracting the H from the hydroxy group, because of its higher acidity than the methyl group (the pK_a values for OH and CH_3 groups are 15–19 and 45–60, respectively).[20]

Reaction barriers and pre-exponential factors derived from the Arrhenius dependence in Figure 3 reflect, in the framework of transition-state theory, the activation enthalpies and entropies required for the formation of O–H scission transition state of CH_3OH. The barriers (Ag: 77 kJ mol^{-1}; Pt: 84 kJ mol^{-1}; Pd 90 kJ mol^{-1}; in Figure 4a) increase with increasing O* binding strength [calculated at low O* coverages, 321 kJ mol^{-1} on Ag(111), 354 kJ mol^{-1} on Pt(111), and 382 kJ mol^{-1} on Pd(111)[9]] following a Brønsted-Evans-Polanyi-type relation, consistent with similar trends reported for H abstraction by chemisorbed oxygen during methane[1a,b] and dimethyl ether[21] oxidation on Pt clusters as well as hydrogen oxidation on metal oxides (Co_3O_4, CuO, MnO_2, Cr_2O_3, Fe_2O_3, V_2O_5, ZnO, and TiO_2),[22] because weakly bound oxygen

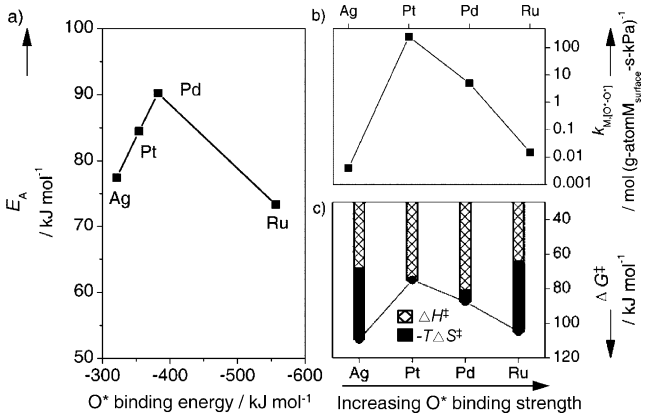

Figure 4. a) Volcano plots of activation barriers (E_A), b) rate constants ($k_{M,[O^*-O^*]}$, 373 K), and c) activation free energies ($\Delta G^{\ddagger}$), which include activation enthalpies ($\Delta H^{\ddagger}$) and entropies (plotted as $-T\Delta S^{\ddagger}$), for CH_3OH oxidative dehydrogenation on O*-covered Ag, Pt, and Pd clusters and RuO_2 clusters measured from this work plotted against the O* binding energy[9] calculated from DFT on closed packed metal surfaces. (O_2-to-CH_3OH ratios of 20–60 for Ag, 10–60 for Pt, 40–60 for Pd, and 20–60 for Ru).

atoms are more basic and thus more effective for H abstraction.[5] On RuO_2 clusters, the barrier is lower (73 kJ mol^{-1}) despite the higher oxygen-binding strength [calculated for O* on Ru(0001) to be 557 kJ mol^{-1} [9]], apparently caused by the different active sites (e.g. Ru^{4+}-O^{2-}) found on oxide than metal surfaces that stabilize the transition state to a larger extent. A similar trend in activation barrier between oxide and O*-covered metal surfaces has been reported for C–H bond activation on Pd (the C–H activation barrier is 61 kJ mol^{-1} on PdO and 158 kJ mol^{-1} on O* covered Pd),[1d] caused predominantly by the stabilization of C–H activation transition state in a tight, four-center [Pd^{2+}-C-H-O^{2-}]$^{+}$ structure on PdO unattainable on O*-saturated Pd surfaces, as the latter lack accessible metal sites.[1d]

Aside from activation barriers ($\Delta E_A < 20$ kJ mol^{-1}), the marked differences in rate constants ($k_{Pt,[O^*-O^*]}/k_{Ag,[O^*-O^*]})^{-1} > 10^5$, 373 K, Figure 4b) are caused to an even larger extent by the differences in activation entropies (Figure 4c). Activation entropies (entropy losses) required to evolve the transition state are essentially negligible on Pt (0 ± 10 J mol^{-1} K^{-1}) and less negative on Pd (-18 ± 10 J mol^{-1} K^{-1}) than on Ag (-110 ± 10 J mol^{-1} K^{-1}) and RuO_2 (-109 ± 10 J mol^{-1} K^{-1}). These values are consistent with the low entropy losses required for the formation of the [CH_3O·-HO*]$^{+}$ transition state on O*-saturated Pt and Pd cluster surfaces, on which the oxygen vacancies are sparse and the CH_3O· fragments interact weakly with one of the O* in O*-O* site pairs and thus retain most of its gas-phase entropy (entropy loss associated with the removal of H from CH_3O-H(g) is estimated to be -2 J mol^{-1} K^{-1} [23]). Activation entropies are significantly more negative on RuO_2 (-109 ± 10 J mol^{-1} K^{-1}), apparently because RuO_2-exposed (110) facets with accessible Ru^{4+} atoms that may stabilize CH_3O fragments at the transition state.[14] The activation entropy on Ag clusters (-110 ± 10 J mol^{-1} K^{-1}) is similar to RuO_2, apparently the presence of oxygen vacancies (exposed Ag atoms) interact with CH_3O fragments at the transition states, consistent with oxygen uptake of less than a monolayer ($O^*_{saturation}/Ag_{surface} = 0.84 \pm 0.05$ at 373 K, Figure 2) at oxygen chemical potentials (30 kPa O_2, without CH_3OH) larger than those during CH_3OH-O_2 catalysis at the same O_2 pressure, because CH_3OH in the latter case acts as O* scavenger to reduce the oxygen chemical potentials. These activation entropy losses indicate that CH_3O fragments interact weakly with O*-saturated Pt and Pd surfaces but more strongly with RuO_2 and Ag surfaces partially covered with O* at the transition state.

In conclusion, first-order rate coefficients for methanol oxidative dehydrogenation are a single-valued function of the operating O_2-to-CH_3OH ratios. This relation appears to be general and results in a kinetic phase diagram that relates kinetic properties to thermodynamic quantities, presented here in terms of the O_2-to-CH_3OH ratio as a surrogate of oxygen chemical potentials and oxygen coverages when oxygen activation is irreversible. Reactive collision frequencies for CH_3OH activation on O*-covered surfaces vary with the oxygen-binding strengths in a classical volcano-type relation because oxygen-binding strengths influence oxygen reactivities as H abstractors and, more importantly, the stability of methoxy fragments at the transition state. The significant differences in entropy losses require for CH_3OH to evolve the transition state, together with those in activation barriers, albeit to a lesser extent, lead to five orders of variation in rate coefficients at 373 K.

Experimental Section

Supported metal clusters (1.0 wt% Ag, Pt, Pd, and Ru) were prepared by incipient wetness impregnation of SiO_2 (330 m^2 g^{-1}, 0—75 μm) with an aqueous solution of the respective precursors [$AgNO_3$, $Pt(NH_3)_4(NO_3)_2$, $Pd(NO_3)_2$, and $Ru(NO)(NO_3)_3$]. The SiO_2 samples impregnated with Ag, Pt, and Pd were treated in ambient air at 353 K for 24 h and then in flowing dry air (Linde, 99.99%, 0.3 cm^3 g^{-1} s^{-1}, 0.033 K s^{-1}) at 773 K (for Ag) or 673 K (for Pt and Pd) for 5 h, followed by treating in 5% H_2/He (Linde certified, 0.3 cm^3 g^{-1} s^{-1}, 0.033 K s^{-1}) at 673 K for 1 h. SiO_2 impregnated with Ru was treated in ambient air at 353 K for 24 h and in 5% H_2/He (0.4 cm^3 g^{-1} s^{-1}, 0.033 K s^{-1}) at 623 K for 3 h. The dispersions of metal clusters were determined from volumetric adsorption methods based on the uptakes of strongly chemisorbed H_2 (313 K for Pt and Ru) or O_2 (313 K for Pd or 433 K for Ag). Average cluster sizes were estimated from these dispersion values by assuming hemispherical cluster shapes. The chemical state of metal clusters was determined by isothermal volumetric oxygen uptakes at 373 K. CH_3OH oxidative dehydrogenation rates were measured in a tubular flow reactor (Quartz, 8.0 mm ID) that contains metal clusters (0.05–250 mg 1.0 wt% M/SiO_2, where M = Pt, Pd, Ru, or Ag) diluted extensively with silica (285 mg) at intra- and interpellet scales to eliminate transport corruptions, confirmed from measured rates and selectivities unaffected by further dilutions.[5] Prior to rate measurements, the samples were treated in flowing H_2 (Linde, 99.99%) at 623 K for 1 h. All gases (He, 5.5% O_2/He, O_2) were independently controlled by electronic mass flow controllers and CH_3OH (Sigma Aldrich, 99.8%) was introduced with a syringe infusion pump. Reactants and products were analyzed by an online micro gas chromatography (Varian CP-4900) equipped with HP-PLOT U and Mol Sieve 5A columns, both of which were connected to thermal conductivity detectors.

Received: May 13, 2014
Revised: July 28, 2014
Published online: September 15, 2014

Keywords: heterogeneous catalysis · methanol · oxidation · oxygen chemical potential · periodic reactivity

[1] a) Y.-H. Chin, C. Buda, M. Neurock, E. Iglesia, *J. Am. Chem. Soc.* **2011**, *133*, 15958 – 15978; b) M. García-Diéguez, Y.-H. Chin, E. Iglesia, *J. Catal.* **2012**, *285*, 260 – 272; c) Y.-H. Chin, E. Iglesia, *J. Phys. Chem. C* **2011**, *115*, 17845 – 17855; d) Y.-H. Chin, C. Buda, M. Neurock, E. Iglesia, *J. Am. Chem. Soc.* **2013**, *135*, 15425 – 15442; e) B. M. Weiss, E. Iglesia, *J. Phys. Chem. C* **2009**, *113*, 13331 – 13340; f) B. M. Weiss, E. Iglesia, *J. Catal.* **2010**, *272*, 74 – 81; g) B. M. Weiss, N. Artioli, E. Iglesia, *ChemCatChem* **2012**, *4*, 1397 – 1404; h) A. Ishikawa, E. Iglesia, *J. Catal.* **2007**, *252*, 49 – 56; i) M. Ojeda, B.-Z. Zhan, E. Iglesia, *J. Catal.* **2012**, *285*, 92 – 102; j) A. D. Allian, K. Takanabe, K. L. Fujdala, X. Hao, T. J. Truex, J. Cai, C. Buda, M. Neurock, E. Iglesia, *J. Am. Chem. Soc.* **2011**, *133*, 4498 – 4517; k) Y. H. Chin, C. Buda, M. Neurock, E. Iglesia, *J. Catal.* **2011**, *283*, 10; l) M. García-Diéguez, E. Iglesia, *J. Catal.* **2013**, *301*, 198 – 209.

[2] S. Y. Yu, J. A. Biscardi, E. Iglesia, *J. Phys. Chem. B* **2002**, *106*, 9642 – 9648.

[3] a) M. Boudart, *Catal. Lett.* **1989**, *3*, 111 – 115; b) M. P. V. Temkin, *Russ. J. Phys. Chem. A* **1939**, *13*, 851; c) A. Logadottir, T. H. Rod, J. K. Nørskov, B. Hammer, S. Dahl, C. J. H. Jacobsen, *J. Catal.* **2001**, *197*, 229 – 231.

[4] G. Ketteler, D. F. Ogletree, H. Bluhm, H. Liu, E. L. D. Hebenstreit, M. Salmeron, *J. Am. Chem. Soc.* **2005**, *127*, 18269 – 18273.

[5] W. Tu, Y.-H. Chin, *J. Catal.* **2014**, *313*, 55 – 69.

[6] a) J. Rossmeisl, P. Ferrin, G. A. Tritsaris, A. U. Nilekar, S. Koh, S. E. Bae, S. R. Brankovic, P. Strasser, M. Mavrikakis, *Energy Environ. Sci.* **2012**, *5*, 8335 – 8342; b) P. Ferrin, M. Mavrikakis, *J. Am. Chem. Soc.* **2009**, *131*, 14381 – 14389; c) P. Ferrin, A. U. Nilekar, J. Greeley, M. Mavrikakis, J. Rossmeisl, *Surf. Sci.* **2008**, *602*, 3424 – 3431.

[7] J. L. C. Fajín, M. N. D. S. Cordeiro, F. Illas, J. R. B. Gomes, *J. Catal.* **2014**, *313*, 24 – 33.

[8] a) F. Viñes, A. Vojvodic, F. Abild-Pedersen, F. Illas, *J. Phys. Chem. C* **2013**, *117*, 4168 – 4171; b) T. Bligaard, J. K. Nørskov, S. Dahl, J. Matthiesen, C. H. Christensen, J. Sehested, *J. Catal.* **2004**, *224*, 206 – 217.

[9] R. A. van Santen, M. Neurock, *Molecular Heterogeneous Catalysis*, Wiley, Hoboken, **2002**.

[10] W. E. Bell, M. Tagami, *J. Phys. Chem.* **1963**, *67*, 2432 – 2436.

[11] a) A. C. Lausche, J. S. Hummelshøj, F. Abild-Pedersen, F. Studt, J. K. Nørskov, *J. Catal.* **2012**, *291*, 133 – 137; b) N. López, G. Novell-Leruth, *Phys. Chem. Chem. Phys.* **2010**, *12*, 12217 – 12222.

[12] a) I. E. Wachs, R. J. Madix, *Surf. Sci.* **1978**, *76*, 531 – 558; b) S. Akhter, J. M. White, *Surf. Sci.* **1986**, *167*, 101 – 126; c) N. Kizhakevariam, E. M. Stuve, *Surf. Sci.* **1993**, *286*, 246 – 260.

[13] a) R. B. Barros, A. R. Garcia, L. M. Ilharco, *J. Phys. Chem. B* **2004**, *108*, 4831 – 4839; b) P. Gazdzicki, P. Jakob, *J. Phys. Chem. C* **2010**, *114*, 2655 – 2663.

[14] H. Over, *Chem. Rev.* **2012**, *112*, 3356 – 3426.

[15] D. Mei, L. Xu, G. Henkelman, *J. Phys. Chem. C* **2009**, *113*, 4522 – 4537.

[16] J. Greeley, M. Mavrikakis, *J. Am. Chem. Soc.* **2002**, *124*, 7193 – 7201.

[17] M. N. D. S. Cordeiro, A. S. S. Pinto, J. A. N. F. Gomes, *Surf. Sci.* **2007**, *601*, 2473 – 2485.

[18] S. K. Desai, M. Neurock, K. Kourtakis, *J. Phys. Chem. B* **2002**, *106*, 2559 – 2568.

[19] R. Jiang, W. Guo, M. Li, D. Fu, H. Shan, *J. Phys. Chem. C* **2009**, *113*, 4188 – 4197.

[20] R. J. Fessenden, J. S. Fessenden, *Organic chemistry*, Willard Grant Press, Boston, **1980**.

[21] A. Ishikawa, M. Neurock, E. Iglesia, *J. Am. Chem. Soc.* **2007**, *129*, 13201 – 13212.

[22] G. K. Boreskov in *Catalysis Science and Technology*, *Vol. 3* (Eds.: J. R. Anderson, M. Boudart), Springer, Berlin, **1982**, pp. 72 – 91.

[23] S. W. Benson, *Thermochemical kinetics*, Wiley, New York, **1976**.